2024 15th International Conference on Computing Communication and Networking Technologies (ICCCNT) | 979-8-3503-7024-9/24/$31.00 ©2024 IEEE | DOI: 10.1109/ICCCNT61001.2024.10724785

Multi-component Damage Diagnostics of a Three-phase Induction Machine Through Hurst Exponent Estimates

Kommanaboina Mahender
Dept. of EEE
BITS Pilani, Hyderabad campus
Hyderabad, India
p20230037@hyderabad.bits-pilani.ac.in

Inturi Vamsi
Dept. of Mechanical Engg.
CBIT (A)
Hyderabad, India
vamsismilebox@gmail.com

Sudha Radhika
Dept. of EEE
BITS Pilani, Hyderabad campus
Hyderabad, India
sradhika@hyderabad.bits-pilani.ac.in

G R Sabareesh
Dept. of Mechanical Engg.
BITS Pilani, Hyderabad campus
Hyderabad, India
sabareesh@hyderabad.bits-pilani.ac.in

Siddharth Singh
Dept. of EEE
BITS Pilani, Hyderabad campus
Hyderabad, India
f20202029@hyderabad.bits-pilani.ac.in

Nikhil Damwani
Dept. of EEE
BITS Pilani, Hyderabad campus
Hyderabad, India
f20201769@hyderabad.bits-pilani.ac.in

***Abstract*—The signals collected from an induction motor are frequently non-stationary and aperiodic. Consequently, extracting health indicators sensitive to defects from the raw signals poses a significant challenge during post-processing. In this paper, we illustrate the benefits of using the Hurst exponents for analyzing non-stationary and aperiodic data, particularly in terms of their fault diagnostics and real-time monitoring capabilities. To exemplify this, a multi-component damage diagnostics of a 3-phase induction motor (TIM) by utilizing Hurst exponents as a health indicator. The condition of TIM is assessed across sixteen health states (including multi-component failures), with raw, time-series motor current being collected for analysis. Two approaches, namely, generalized Hurst exponent and R/S analysis are used for estimating the Hurst exponents. Three distinct input datasets from the health indicators (Hurst exponents) for motor current signals are constructed and then undergo feature learning via machine-learning (ML) methods. The effectiveness of the integrated dataset while accomplishing the multi-component defect diagnostics of TIM and yielding better classification accuracies (∼99%) is investigated. Thus, the ability to perform multi-component defect diagnostics and characterize the diverse health scenarios of the TIM with minimal human intervention is demonstrated.**

***Index Terms*—Induction motor, Hurst exponent, Condition monitoring, Multi-component defect, Machine-learning**

I. Introduction

Three-phase induction motors (TIMs) are largely employed in various industrial avenues, including energy generation, manufacturing, transportation, HVAC systems, etc.. These motors operate on three-phase alternating current and employ electromagnetic induction to transform the electrical energy into mechanical energy. Owing to its robust construction, reliability, and ease of maintenance, the TIMs have found extensive applications across various industries [1]. Though TIMs are regarded as reliable and robust industrial machines, they are often subjected to volatile operating conditions, eventually resulting in the production of various stresses (mechanical, electrical, thermal, etc.), which could disrupt the normal running conditions and lead to the nucleation of defects [2]. The defects related to the rotor and bearings of TIM are classified as mechanical faults, whilst the stator-related defects of TIM are classified as electrical faults. The stator defects happen more frequently and are regarded as one of the primary defects of TIMs, as they contribute to 25%-40% of TIM failures [3]. If a stator defect is not detected at its nascent level, it could lead to the generation of secondary faults, such as an increase in coil current and phase-to-phase defects, eventually imposing motor winding deterioration [4]. Therefore, an incipient defect diagnosis is vital in order to reduce the events of catastrophic failures and extending the life span of the TIM. For TIMs, condition monitoring (CM) is been instrumental not only to ensure operational reliability but also to detect failures and the evolution of failures and reduce premature breakdowns. The exploitation of motor current-based CM is crucial as the motor current signals are dynamic, and the existence of defects causes amplitude and distribution modulations. Various researchers have implemented motor current-based CM strategies and investigated the defect diagnostics and severity estimation of TIMs [3]–[5]. As the TIM consists of various sub-components, such as stator, rotor, bearings, shaft, etc., the potential defect-sensitive information (health indicators) exist in the raw motor current signals could obscured due to complex multi-component interactions and background noise.

Numerous signal processing algorithms are being used to recover the relevant health indicator information from the raw motor current signals. Besides, a defect (either stator or rotor) makes the acquired raw motor current signals non-stationary and aperiodic [5]. Multi-domain (time-frequency) analysis techniques are implemented to decompose the raw signals for computing the relevant and defect-sensitive health indicators/features because of their capacity to handle non-stationary signals [6], [7]. Various researchers have implemented the wavelet transform, variational mode decomposition, Hilbert-Huang transform, etc. approaches and computed statistical health indicators/features from the raw signals [6], [7]. However, these approaches require additional computational resources, and each of these algorithms offers unique advantages and has certain limitations while computing the health indicators/features [8]. Therefore, to remain within the context of fault diagnosis, it is necessary to compute an appropriate defect-sensitive health indicator. Hurst exponents are statistical time-domain parameters and have found significant application in various avenues, such as fuel pricing, river flow analysis, stock market analysis, etc. Hurst exponent approach is shown to be a suitable health indicator for handling non-stationary signals as it relies on scale-invariance and self-similarity of the raw signals [9]. Also, because of its fractal behavior, this approach works well with long-range time-series data, which is hardly possible with the multi-domain analysis approaches [8]. Additionally, the Hurst exponent approach offers low-cost computing compared to multi-domain approaches. Usually, the Hurst exponent computed lies in the range of ‘0’ to ‘1’. The Hurst exponent greater than 0.5 (H$>$0.5) indicates persistence, meaning that there exists a positive correlation or long-range correlation among the data points [10]. Similarly, the Hurst exponent with a value less than 0.5 (H$<$0.5) represents an anti-persistence, meaning that there exists a negative correlation or low long-range correlation among the data points [11]. Besides, the Hurst exponent equal to 0.5 (H=0.5) corresponds to a classical Brownian motion, i.e., no correlation in the data [12]. Extracting the Hurst exponent followed by data-driven classification could discern and categorize the diverse health states of the TIM, leading to a remote and effective CM.

II. Experimentation And Methodology

The raw, time-series, three-phase current measurements (I_x, I_y, I_z) are obtained from a 3-phase induction machine (TIM), as depicted in Fig. 1. The experimental test rig is designed to emulate various operational conditions under fault scenarios. The defects are seeded artificially, i.e., by tapping the winding on the stator and rotor individually, and the defective components (stator and rotor together) are installed, resulting in a multi-component defect scenario in the TIM test rig. In this study, a total of sixteen health states/conditions of the TIM, i.e., healthy, stator defect (with four severity levels) and rotor defect (with four severity levels), are considered, refer Table 1. To ensure high fidelity, the data is captured using a NI myDAQ USB6210 multifunction I/O device, boasting a 16-bit analogue input with a sampling rate of 250 kS/s, four digital inputs, and four digital outputs. The three-phase motor current data acquisition is realized with a sampling rate of 10 kHz. For each health scenario of the TIM, three-phase motor current signals $(I_x, I_y \& I_z)$ are captured with 10 kHz sampling frequency, and 500 observations and 1024 data points are acquired for each observation. Thus, for each health state/condition of the TIM, there are 5,12,000 points. The measured raw, time-series, three-phase motor current signals are further subjected to Hurst exponent estimation using generalized Hurst (GenHurst) exponent approach (with q=1, 2, 3, 4 & 5) and range (R/S) analysis.

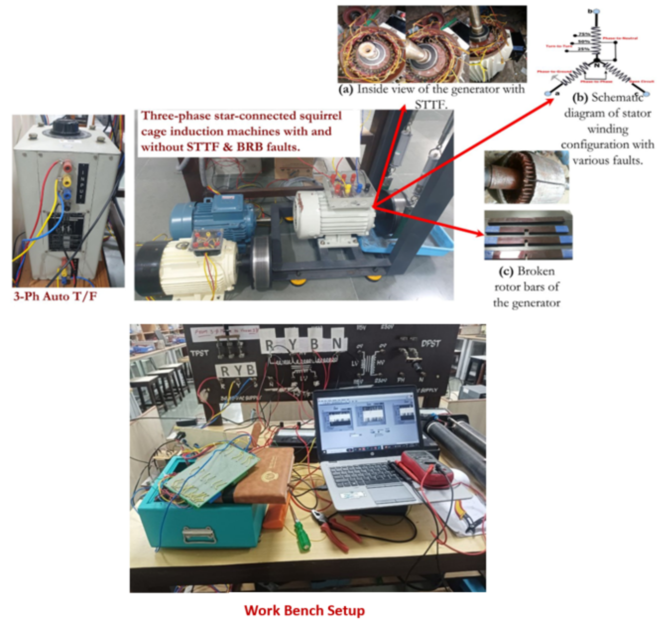

Fig. 1. 3-phase induction motor system considered for damage diagnostics along with the seeded defects.

Three different kinds of datasets from the experimental rig are prepared; in which the dataset I contains the Hurst exponents estimated from the motor current signals through GenHurst approach (with q=1, 2, 3, 4 & 5), which mounts to a order of fifteen rows (5 Hurst exponents of I_x+ I_y+ I_z) and 8000 columns (16 health scenarios * 500 observations). Similarly, the Hurst exponents computed through R/S analysis approach are used for devising the dataset II, whose order is three rows (3 Hurst exponents of $I_x, I_y \& I_z$) and 8000 columns (16 health scenarios * 500 observations). In order to obtain input dataset III, the individual Hurst exponents devised through generalized Hurst exponent approach (input dataset I) and R/S analysis approach are (input dataset II) are combined. Therefore, the input feature dataset III mounts to have 18 rows (6 Hurst exponents of I_x+ I_y+ I_z) and 8000 columns (16 health scenarios * 500). Ultimately, all the formulated input feature/health indicator dataset is fed into various machine-learning (ML) algorithms to implement better feature learning. Finally, the ability of the input health indicator set to yield favorable health state classification/demarcation of the TIM is investigated.

III. Results and Discussion

A. Generalized Hurst exponent

The Hurst exponent measures the persistence in the long-range datasets based on self-similarity or autocorrelations, thus it is referred as the index of statistical persistence/dependence

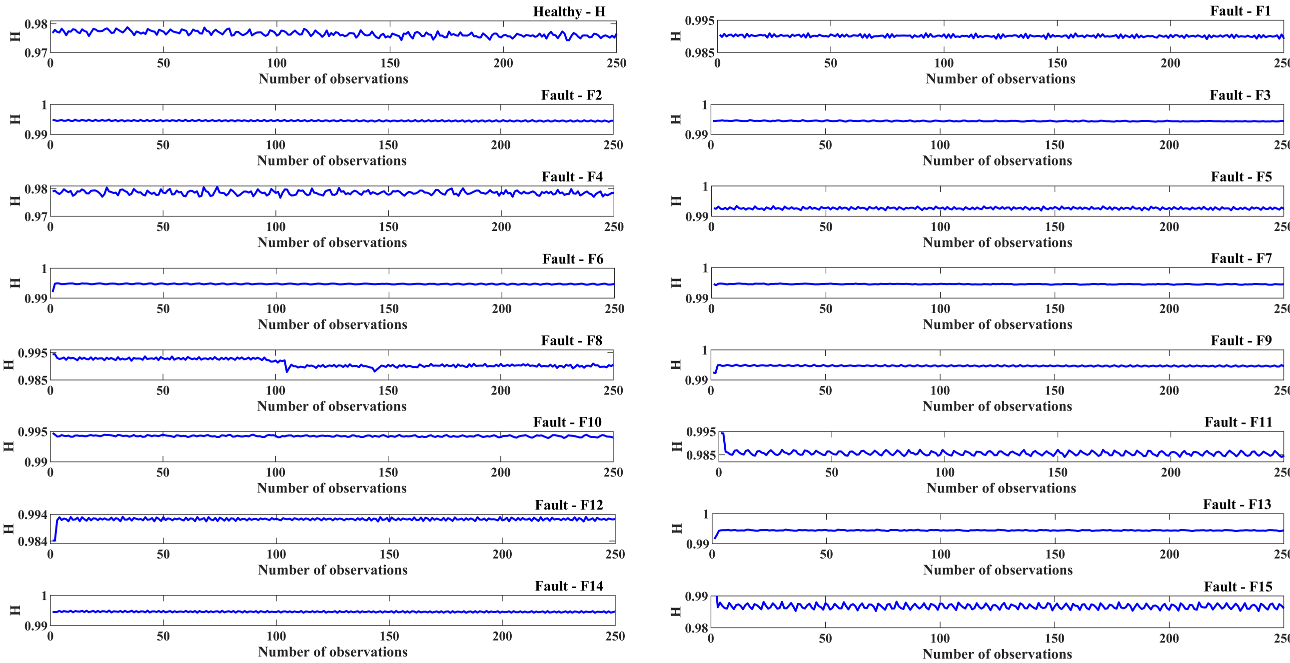

Fig. 2. A glimpse of GenHurst exponent computed with ‘q’ = 2 from the motor current signals of the TIM system.

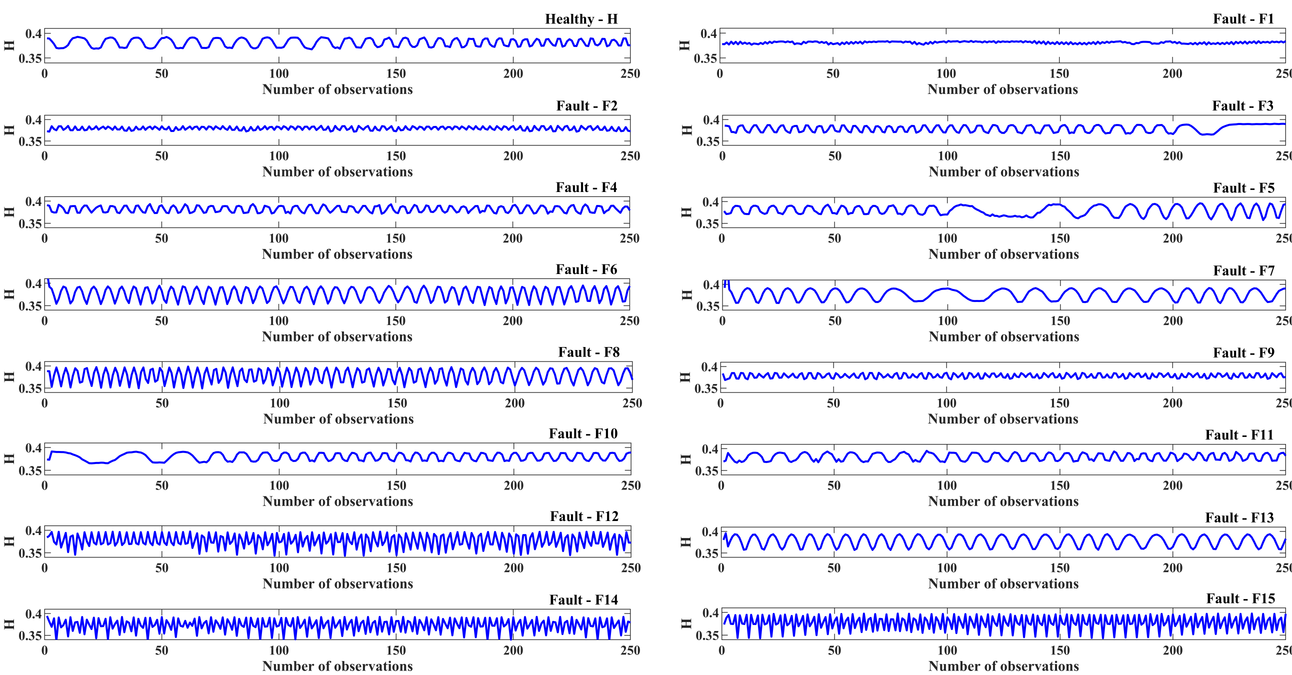

Fig. 3. A glimpse of Hurst exponent computed through R/S analysis from the motor current signals of the TIM system.

TABLE I
DESCRIPTION ABOUT THE HEALTH SCENARIOS OF THE 3-PHASE INDUCTION MOTOR CONSIDERED

Type of defect	Stator damage (25% severity)	Stator damage (50% severity)	Stator damage (75% severity)	No stator damage (0% severity)
Rotor damage (25% severity)	Defect 1 - D1	Defect 2 - D2	Defect 3 - D3	Defect 4 - D4
Rotor damage (50% severity)	Defect 5 - D5	Defect 6 - D6	Defect 7 - D7	Defect 8 - D8
Rotor damage (75% severity)	Defect 9 - D9	Defect 10 - D10	Defect 11 - D11	Defect 12 - D12
No rotor damage (0% severity)	Defect 13 - D13	Defect 14 - D14	Defect 15 - D15	Healthy - H

of the signal [13]. Among the many techniques used for calculating the scaling properties of a time-series signal, the equation proposed by [14] is used in this current work to compute the generalized Hurst exponent. Equation 1 quantifies the stochastic evolution of '$\Delta(t)$' to the GenHurst. Where the correlation across the simultaneous data points $\Delta(ti+1)$ and $\Delta(ti)$ is expressed by '$C_q(\tau)$', time instant 't' and the resolution at 't' is 'ν', i.e., t = $=\nu, 2\nu, 3\nu \ldots\ldots T$. Thus, the statistical properties of the time series signal M(t) at stationary time instants/steps 't' with a total time of observation (T) are examined. In the current work, the first five orders of moments ('q' values from 1 to 5) are considered for examining the scaling function of qH (q). The Hurst exponent greater than 0.5 (H>0.5) indicates a positive correlation, and the Hurst exponent with a value less than 0.5 (H<0.5) represents a low long-range correlation among the data points [11]. Thus, the variation in the Hurst exponent (a sudden rising spike or a declining drift) of the acquired signal indicates an unprecedented event in the system [15]. The computed GenHurst exponents for the considered health scenarios of the TIM are shown in Fig. 2.

$$C_q(\tau) = \frac{<\mid \Delta(t+\tau) - \Delta(t) \mid^q>}{<\mid \Delta(t) \mid^q>} \sim \left(\frac{\tau}{\nu}\right)^{qH(q)} \tag{1}$$

B. R/S analysis

This approach is capable of tracking the variations of long range time-series data. Initially, the time-series signal under investigation 'M(t)' is segmented into a series of sub-signals (ν) having a length of 'k' for calculating the R/S. The mean values (m) pertaining to each sub-signal (ν) are calculated, and the signal gets normalized '$N_(n,k)(t)$' by removing the mean values from each of the sub-signals (ν) as shown in Eq. 2. Later, the cumulative mean fluctuation '$S_1(k)$' is compiled using Eq. 3 followed by the calculation of range '$X(k)$' of time-series signal using the Eq. 4. Further, the Eq. 4 is divided with the Eq. 3 for obtaining the rescale range of each sub-signal. Finally, by fitting the power law as shown in Eq. (5), the Hurst exponent is calculated. Fig. 3 illustrates the Hurst exponents computed for various health state/condition of the TIM through R/S approach.

$$N_{n,k}(t) = M_{n,k}(t) - m_{n,k} \tag{2}$$

$$\sqrt{\frac{1}{k}\sum_{1}^{k} S^2(\nu,k)} \tag{3}$$

$$X(k) = max\left(N_{1,k}, N_{2,k}, N_{3,k}, \ldots\ldots\ldots N_{\nu,k}\right) - min\left(N_{1,k}, N_{2,k}, N_{3,k}, \ldots\ldots\ldots N_{\nu,k}\right) \tag{4}$$

$$E\left[\frac{X(k)}{S_1(k)}\right] = C_n^H \tag{5}$$

Three different kinds of datasets are formulated; the dataset I contains the Hurst exponents estimated from the motor current signals through GenHurst approach (with q=1, 2, 3, 4 & 5). Similarly, the Hurst exponents computed through R/S analysis approach are used for devising the dataset II. In order to obtain dataset III, the individual Hurst exponents devised through generalized Hurst exponent approach (input dataset I) and R/S analysis approach are (dataset II) are combined. Ultimately, all the formulated input feature/health indicator dataset is fed into various ML classifiers (decision tree, Naïve-Bayes, support vector machine, k-nearest neighbors & random forest) to implement better feature learning followed by health scenario identification.

C. ML-based health state identification

ML algorithms perform non-liner operations on the given input feature vector set (health indicator set) to achieve better feature learning followed by mapping with the output (health state/scenario) class. Unlike deep-learning algorithms, ML algorithms can handle small and limited labelled feature vector datasets [16]. Support Vector Machine (SVM) operates by identifying the ideal hyperplane that distinguishes between various labels/classes exist in the dataset [17]. The K-Nearest Neighbours (KNN) algorithm falls within the category of instance-based algorithms because it does not explicitly learn a model. The KNN algorithm operates by memorizing the training dataset during the training phase and making predictions between new instances and the stored data. The decision tree (DT) is an inverted tree-based algorithm works on the strategy of information gain [16]. The Random Forest (RF) classifier algorithm functions by constructing multiple decision trees, a method referred to as bootstrapping [17]. The three datasets (I, II & III) are supplied as input to all the above-mentioned ML algorithms individually for achieving the multi-component

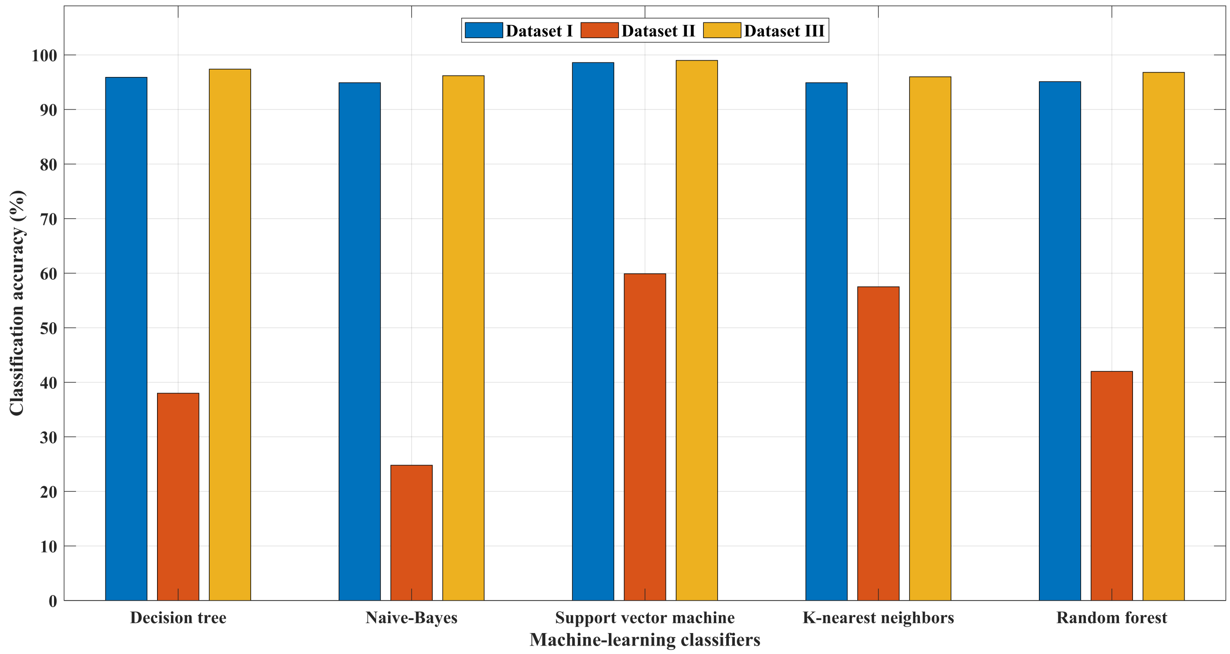

Fig. 4. Classification accuracies obtained through various ML classifiers pertaining to various input datasets.

damage diagnostics. Training is done with the 80% of the data and 5-fold cross-validation is implemented. The obtained classification accuracies pertaining to each of the datasets are shown in Fig. 4.

It can be observed that, during the multi-categorical classification, the Hurst exponents computed through generalized Hurst approach (dataset I) resulted to favourable classification accuracies. The achieved classification accuracies are 95.9%, 94.9%, 98.6% and 94.9% for DT, Naïve-Bayes, SVM and KNN classifiers, respectively. This could be due that, the generalized Hurst approach sensitive towards the fractal and self-similarity behaviour exist in the time-series data computed at various orders of moment, which eventually leads to a better discrimination across the considered health scenarios of the TIM. Besides, when compared with the dataset I, the dataset II has yielded to reduced classification accuracies while distinguishing considered health scenarios of the TIM. This could be due to the fact that, the R/S analysis emphasis towards the self-similarity and scale-invariance behaviour of the data considered. It is worth to observe that, the integration of individual Hurst exponents, i.e., input dataset III has resulted to an improved classification accuracy. As the dataset III holds the advantages of individual self-similarity and fractal behaviour exist at various sub-bands of the time-series data under investigation. Thus, the dataset III yields to better classification accuracies of 97.4%, 96.2%, 99%, 96% and 96.8% for DT, Naïve-Bayes, SVM, KNN and RF classifiers, respectively. It's notable that the SVM classifier has provided superior classification accuracies across most scenarios, as the SVM algorithm demonstrates superior generalization property when handling smaller datasets [18], refer Fig. 4. Therefore, the proposed health indicator (Hurst exponent) itself can perform the multi-component defect diagnostics of TIM, enhancing the scope of intelligent defect diagnostics.

IV. Conclusion

This research work attempts to conduct fault diagnostics on a 3-phase induction motor (TIM) utilizing a health indicator based on Hurst exponents. A total of sixteen health states/scenarios (including multi-component defects) are considered, and the raw time-series motor current are captured from a TIM rig. The Hurst exponents are estimated through two different approaches; GenHurst (q= 1, 2, 3, 4 & 5) and R/S analysis from the captured motor-current signals pertaining to each health state/scenario. Three datasets are formulated; in which dataset I contains the Hurst exponents extracted through GenHurst approach. The Hurst exponents estimated using R/S analysis approach constitute dataset II, while dataset III incorporates the fusion of these Hurst exponents. These datasets are fed into ML algorithms (DT, Naïve-Bayes, SVM and KNN) for feature learning and subsequent classification. The below conclusions are drawn:

- The dataset III has registered higher classification accuracies than the datasets I and II, as it holds the advantages of individual self-similarity and fractal behavior exist at various sub-bands of the time-series data and thus, it has resulted to favorable classification accuracies.
- The SVM classifier has provided superior classification accuracies across most scenarios, as the SVM algorithm demonstrates superior generalization property when handling smaller datasets.
- The proposed approach overcomes with the issues related to data loss, as the health indicator (Hurst exponent) is devised from raw, time-series motor-current signals.

Thus, the health indicator (Hurst exponent) itself can perform the multi-component defect diagnostics of TIM along with discriminating across the health scenarios of the TIM.

REFERENCES

[1] Vo, T. T., Liu, M. K., & Tran, M. Q. (2024). Harnessing attention mechanisms in a comprehensive deep learning approach for induction motor fault diagnosis using raw electrical signals. Engineering Applications of Artificial Intelligence, 129, 107643.

[2] Noussaiba, L. A. E., & Abdelaziz, F. (2024). ANN-based fault diagnosis of induction motor under stator inter-turn short-circuits and unbalanced supply voltage. ISA transactions, 145, 373-386.

[3] Vitor, A. L., Goedtel, A., Junior, S. B., Bazan, G. H., Castoldi, M. F., & Souza, W. A. (2023). Induction motor short circuit diagnosis and interpretation under voltage unbalance and load variation conditions. Expert Systems with Applications, 224, 119998.

[4] Verma, A. K., Nagpal, S., Desai, A., & Sudha, R. (2021). An efficient neural-network model for real-time fault detection in industrial machine. Neural Computing and Applications, 33, 1297-1310.

[5] Almounajjed, A., Sahoo, A. K., & Kumar, M. K. (2021). Diagnosis of stator fault severity in induction motor based on discrete wavelet analysis. Measurement, 182, 109780.

[6] Inturi, V., Pratyush, A. S., & Sabareesh, G. R. (2021). Detection of local gear tooth defects on a multistage gearbox operating under fluctuating speeds using DWT and EMD analysis. Arabian Journal for Science and Engineering, 46(12), 11999-12008.

[7] Mohanty, S., Gupta, K. K., & Raju, K. S. (2018). Hurst based vibro-acoustic feature extraction of bearing using EMD and VMD. Measurement, 117, 200-220.

[8] Inturi, V., Balaji, S. V., Gyanam, P., Pragada, B. P. V., Geetha Rajasekharan, S., & Pakrashi, V. (2023). An integrated condition monitoring scheme for health state identification of a multi-stage gearbox through Hurst exponent estimates. Structural Health Monitoring, 22(1), 730-745.

[9] Fan, Y., Tao, M., Su, J., & Wang, L. (2020). Weak target detection based on whole-scale Hurst exponent of autoregressive spectrum in sea clutter background. Digital Signal Processing, 101, 102714.

[10] Aldea, R., & Tărniceriu, D. (2013, October). Estimating the Hurst exponent in motor imagery-based brain computer interface. In 2013 7th Conference on Speech Technology and Human-Computer Dialogue (SpeD) (pp. 1-6). IEEE.

[11] Sommers, B. N., & Davis, B. L. (2021). Examining feedback mechanisms of postural control in Chiari Malformation by average wavelet coefficient decomposition and the Hurst exponent. Gait & Posture, 88, 280-285.

[12] Mosqueda-Herrera, A., Martinez-Peon, D., Gomez-Sanchez, L., Ramirez-Sosa, M. I., Delfin-Prieto, S., & Benavides-Bravo, F. G. (2020, October). Characterization of Kinesthetic Motor Imagery paradigm for wrist and forearm using an algorithm based on the Hurst Exponent and Variogram. In 2020 IEEE International Conference on Systems, Man, and Cybernetics (SMC) (pp. 3683-3688). IEEE.

[13] Gómez-Águila, A., Trinidad-Segovia, J. E., & Sánchez-Granero, M. A. (2022). Improvement in Hurst exponent estimation and its application to financial markets. Financial Innovation, 8(1), 86.

[14] Di Matteo, T., Aste, T., & Dacorogna, M. M. (2003). Scaling behaviors in differently developed markets. Physica A: Statistical Mechanics and its Applications, 324(1-2), 183-188.

[15] Domino, K. (2011). The use of the Hurst exponent to predict changes in trends on the Warsaw Stock Exchange. Physica A: Statistical Mechanics and its Applications, 390(1), 98-109.

[16] Inturi, V., Ritik Sachin, P., & Sabareesh, G. R. (2020). Supervised feature selection methods for fault diagnostics at different speed stages of a wind turbine gearbox. In Modelling, Simulation and Intelligent Computing: Proceedings of MoSICom 2020 (pp. 478-486). Springer Singapore.

[17] Wei, Y., Yang, Y., Xu, M., & Huang, W. (2021). Intelligent fault diagnosis of planetary gearbox based on refined composite hierarchical fuzzy entropy and random forest. ISA transactions, 109, 340-351.

[18] Liu, R., Yang, B., Zio, E., & Chen, X. (2018). Artificial intelligence for fault diagnosis of rotating machinery: A review. Mechanical Systems and Signal Processing, 108, 33-47.